Radiology

ORIGINAL RESEARCH • VASCULAR AND INTERVENTIONAL RADIOLOGY

Transarterial Embolization Modulates the Immune Response within Target and Nontarget Hepatocellular Carcinomas in a Rat Model

David J. Tischfield, MD, PhD • Alexey Gurevich, MD, MS* • Omar Johnson, BS • Isabela Gatmaytan, AB • Gregory J. Nadolski, MD, MS • Michael C. Soulen, MD • David E. Kaplan, MD, MS • Emma Furth, MD • Stephen J. Hunt, MD, PhD • Terence P. F. Gade, MD, PhD*

From the Penn Image-Guided Interventions Laboratory (D.J.T., A.G., O.J., I.G., G.J.N., S.J.H., T.P.F.G.), Department of Radiology (D.J.T., O.J., G.J.N., M.C.S., S.J.H., T.P.F.G.), and Department of Pathology (E.F.), Hospital of the University of Pennsylvania, 3400 Spruce St, Philadelphia, PA 19104; Division of Gastroenterology and Hepatology (D.E.K.) and Department of Cancer Biology (T.P.F.G.), Perelman School of Medicine at the University of Pennsylvania, Philadelphia, Pa; and Gastroenterology Section, Corporal Michael J. Crescenz Veterans Affairs Medical Center, Philadelphia, Pa (D.E.K.). Received April 21, 2021; revision requested June 30; revision received October 12; accepted October 28. **Address correspondence to** T.P.F.G. (e-mail: *tgade@pennmedicine.upenn.edu*).

Supported by the Society of Interventional Oncology Immuno-Oncology/Interventional Oncology grant program and the National Institutes of Health (grants R01CA234005 and DP5OD021391).

* D.J.T. and A.G. contributed equally to this work.

Conflicts of interest are listed at the end of this article.

See also the editorials by Kennedy et al and by White in this issue.

Radiology 2022; 303:215–225 • https://doi.org/10.1148/radiol.211028 • Content codes: GI MR IR

Background: Transarterial embolization (TAE) is the most common treatment for hepatocellular carcinoma (HCC); however, there remain limited data describing the influence of TAE on the tumor immune microenvironment.

Purpose: To characterize TAE-induced modulation of the tumor immune microenvironment in a rat model of HCC and identify factors that modulate this response.

Materials and Methods: TAE was performed on autochthonous HCCs induced in rats with use of diethylnitrosamine. CD3, CD4, CD8, and FOXP3 lymphocytes, as well as programmed cell death protein ligand-1 (*PD-L1*) expression, were examined in three cohorts: tumors from rats that did not undergo embolization (control), embolized tumors (target), and nonembolized tumors from rats that had a different target tumor embolized (nontarget). Differences in immune cell recruitment associated with embolic agent type (tris-acryl gelatin microspheres [TAGM] vs hydrogel embolics) and vascular location were examined in rat and human tissues. A generalized estimating equation model and *t*, Mann-Whitney *U*, and χ^2 tests were used to compare groups.

Results: Cirrhosis-induced alterations in CD8, CD4, and CD25/CD4 lymphocytes were partially normalized following TAE (CD8: 38.4%, CD4: 57.6%, and CD25/CD4: 21.1% in embolized liver vs 47.7% [$P = .02$], 47.0% [$P = .01$], and 34.9% [$P = .03$], respectively, in cirrhotic liver [36.1%, 59.6%, and 4.6% in normal liver]). Embolized tumors had a greater number of CD3, CD4, and CD8 tumor-infiltrating lymphocytes relative to controls (191.4 cells/mm^2 vs 106.7 cells/mm^2 [$P = .03$]; 127.8 cells/mm^2 vs 53.8 cells/mm^2 [$P < .001$]; and 131.4 cells/mm^2 vs 78.3 cells/mm^2 [$P = .01$]) as well as a higher *PD-L1* expression score (4.1 au vs 1.9 au [$P < .001$]). A greater number of CD3, CD4, and CD8 lymphocytes were found near TAGM versus hydrogel embolics (4.1 vs 2.0 [$P = .003$]; 3.7 vs 2.0 [$P = .01$]; and 2.2 vs 1.1 [$P = .03$], respectively). The number of lymphocytes adjacent to embolics differed based on vascular location (17.9 extravascular CD68$^+$ peri-TAGM cells vs 7.0 intravascular [$P < .001$]; 6.4 extravascular CD68$^+$ peri-hydrogel embolic cells vs 3.4 intravascular [$P < .001$]).

Conclusion: Transarterial embolization–induced dynamic alterations of the tumor immune microenvironment are influenced by underlying liver disease, embolic agent type, and vascular location.

Online supplemental material is available for this article.

Hepatocellular carcinoma (HCC) is the second leading cause of cancer-associated death worldwide and the fifth leading cause of cancer death in the United States (1,2). Transarterial chemoembolization (TACE) and immunotherapy are first-line therapies for patients with intermediate and advanced HCC, respectively. Although TACE and immunotherapy have proven survival benefits in select patient populations, local and distant recurrences are common (3,4). To overcome these limitations, existing treatment paradigms must continue to evolve, and there is growing interest in integrating TACE and immunomodulators for combination therapy.

Multiple locoregional therapies, including embolotherapies, have shown the potential for immune activation (5–7). TACE represents a particularly promising candidate for this approach, given the potential for immune stimulation by means of the large-scale release of tumor-associated antigens following ischemia-induced cell death (7). Although clinical trials combining TACE with immune checkpoint inhibitors (ICIs) are ongoing (8,9), there has been limited characterization of embolotherapy-induced immune alterations that is essential for informing the integration of therapeutic immunomodulation into clinical protocols (10,11). Fundamental questions remain to be answered,

Abbreviations

HCC = hepatocellular carcinoma, ICI = immune checkpoint inhibitors, IHC = immunohistochemistry, ISH = in situ hybridization, PD-L1 = programmed cell death protein ligand-1, TACE = transarterial chemoembolization, TAE = transarterial embolization, TAGM = tris-acryl gelatin microspheres, TIL = tumor-infiltrating lymphocyte

Summary

Transarterial embolization–induced alterations in the tumor immune microenvironment are influenced by underlying liver disease, embolic agent type, and vascular location and result in increased programmed cell death protein ligand-1 expression.

Key Results

- Transarterial embolization normalized proportions of CD8 and CD4 lymphocytes (38.4% [CD8] and 57.6% [CD4] in embolized liver vs 47.7% [$P = .02$] and 47.0% [$P = .01$] in cirrhotic liver [36.1% and 59.6% in normal liver]).
- Embolized tumors had higher programmed cell death protein ligand-1 expression than nonembolized controls (4.1 au vs 1.9 au [$P < .001$]).
- Tris-acryl gelatin microspheres extravasated at higher rates than hydrogel embolics (87% vs 41% [$P < .001$]) and recruited more peri-embolic CD4 and CD8 lymphocytes (3.7 vs 2.0 [$P = .01$] and 2.2 vs 1.1 [$P = .03$], respectively).

including the ability of embolotherapy to enhance the infiltration and activation of immune cell populations in target and nontarget tumors.

The paucity of studies characterizing embolotherapy-related immune responses issues from two primary challenges. These include the lack of standardized embolization techniques and limitations in animal models that faithfully recapitulate the hallmark features of HCC while enabling the recapitulation of clinical embolotherapy protocols. HCC generally arises from a background of chronic liver disease or cirrhosis, which profoundly alters the immunobiologic characteristics and architecture of the liver (12,13). It is therefore critical that animal models recapitulate the immune microenvironment in which HCC arises as well as the changes in scaffolding and vasculature that accompany chronic liver disease. Complicating matters further is the inconsistent use of standardized embolic agents across preclinical and clinical studies. Depending on their physical and chemical properties, different embolic agents have varying propensities to extravasate outside of the vasculature and elicit inflammatory tissue reactions (14–16)—properties that may influence the overall immune response to TACE.

An improved understanding of the nature and mechanisms of immune activation in the setting of embolization is required to design more effective treatment strategies that leverage the TACE-induced modulation of the tumor environment to achieve an optimal antitumor immune response. The purpose of this study was to characterize transarterial embolization (TAE)–induced modulation of the immune microenvironment within autochthonous HCCs induced in rats and to identify factors that modulate this response.

Materials and Methods

The experimental schema and animal cohorts are described in Figure 1.

Autochthonous Rat Model of HCC and TAE

Animal studies were conducted in accordance with institutionally approved protocols adhering to Institutional Animal Care and Use Committee guidelines. Briefly, autochthonous HCCs were induced in male Wistar rats weighing 300–400 g (Charles River Laboratories) with use of ad libitum oral administration of 0.01% diethylnitrosamine for 12 weeks, which induces liver tumors through sequential progression of hepatitis, cirrhosis, and carcinogenesis (17). Rats with at least one tumor measuring 0.5–1.0 cm in maximum diameter on T2-weighted MRI scans (Agilent 4.7-T 40-cm horizontal bore MRI; repetition time minimum, 1.4 seconds [respiratory-gated]; echo time, 59.1 msec) were selected for the experiment. Animals were only included if they had at least one targetable lesion. Transarterial access was gained through ventral tail artery or transfemoral approach (18,19). With use of fluoroscopic guidance, the artery feeding the target tumor was selectively catheterized and embolized with 0.2 mL of 40–120 μm tris-acryl gelatin microspheres (TAGM) (Embosphere, Merit Medical) or 70–150 μm hydrogel embolics (LUMI beads, BTG) suspended in 1 mL iopamidol contrast medium (Isovue 370, Bracco) (17). Pre- and post-embolization arteriography was performed using an Angiostar Plus or Cios imaging system (Siemens), and stasis of contrast material within the target vessel was confirmed in embolized animals (by S.J.H., O.J., A.G., or T.P.F.G., with 16, 3, 3, and 16 years of experience, respectively). Ten rats were embolized with hydrogel embolics (two rats were euthanized 2 days after embolization and eight rats were euthanized 7 days after embolization). The remaining 38 rats were embolized with TAGM.

Eighteen rats were used for flow cytometry experiments and collected for analysis 7 days following embolization. A total of 48 rats were used for immunohistochemistry (IHC) and in situ hybridization (ISH) experiments and collected for analysis 2, 7, or 12 days following embolization. For IHC and ISH experiments, additional rats were added to cohorts collected at later time points to compensate for attrition due to tumors developing after treatment. Nontarget tumors in rats that had a different target tumor embolized were also collected to determine whether TAE influenced tumor lymphocyte infiltration in these tumors. Nontarget tumors were collected at the time of necropsy at either 2, 7, or 12 days after embolization. Time points for tissue harvest were based on prior studies demonstrating peak T-cell response in peripheral blood 14 days following locoregional therapies (20,21).

Tissue Preparation and Histologic Examination

Treated and untreated tumors were harvested from rats following euthanasia in accordance with institutionally approved protocols. Tumors were hemisected, fixed overnight in formalin, and dehydrated with 70% alcohol before paraffinization. The pathologic diagnosis of HCC was confirmed on 4-μm-thick hematoxylin and eosin–stained sections by a hepatobiliary pathologist with 35 years of experience in evaluating HCC (E.F.). One central section per tumor was used for cell counting.

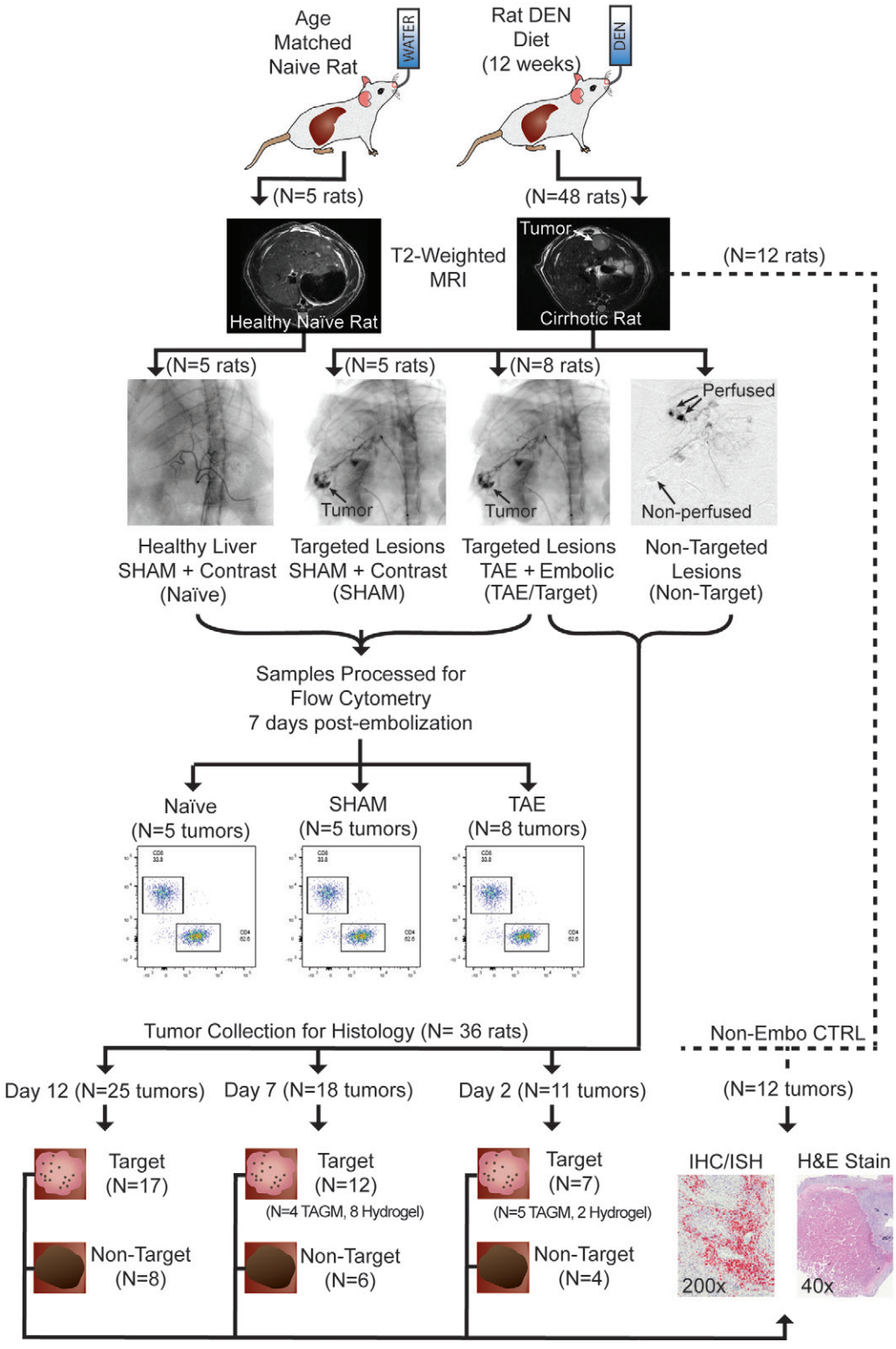

Figure 1: Experimental flowchart. Chemically induced autochthonous hepatocellular carcinomas were generated in Wistar rats, and tumor development was monitored using T2-weighted MRI. Tumors reaching 0.5–1 cm in maximum transverse diameter were treated with transarterial embolization (TAE). At selected post-TAE time points, samples were collected for analysis with either flow cytometry or immunohistochemistry (IHC)/in situ hybridization (ISH). Flow cytometry was performed on three different groups: liver samples from healthy diethylnitrosamine (DEN)–naive rats treated with sham embolization (naive), sham-treated tumors (SHAM), and embolized tumors (TAE group). Histologic examination (IHC, ISH, hematoxylin and eosin [H&E] staining) was performed on three different groups: tumors from rats that did not undergo embolization (non-embo CTRL), embolized tumors (target or TAE), and nonembolized tumors from rats that had a different target tumor embolized (nontarget). Hydrogel = hydrogel embolics, TAGM = tris-acryl gelatin microspheres.

IHC, Immunofluorescence, and ISH

Standard IHC and immunofluorescence protocols were used to stain tissues fixed in formalin and embedded in paraffin (by D.J.T. [with 16 years of experience], A.G., O.J., and I.G. [with 3 years of experience]). ISH for CD4 and programmed cell death protein ligand-1 (PD-L1) (a predictive marker of response to ICIs and enriched in HCC [22,23]) was performed by D.J.T. on sections fixed in formalin and embedded in paraffin with use of RNAscope 2.5 HD Brown Reagent Kit in combination with RNAscope Probe-Rn-CD4 and RNAscope Probe-NPR-0002409-PDL1 (Advanced Cell Diagnostics) according to the manufacturer's instructions. See Appendix E1 (online) for additional details.

Flow Cytometry

Rat tissue, including spleen, liver, target tumor, and nontarget tumor, was prepared for flow cytometry (by A.G. and O.J.) (Fig 2) based on established protocols (24) (Appendix E1 [online]).

Cell Counting and Image Analysis

Cell counting (ISH and IHC pertaining to Figs 3–5) was performed using ImageJ version 1.53g (National Institutes of Health) in a blinded fashion, wherein digitally scanned slides were anonymized before counting (by D.J.T., A.G., and I.G.). with use of a unique identifier. Because the proportion of tumor-infiltrating lymphocytes (TILs) found within connective tissue and vasculature (stromal compartment), versus embedded within the tumor parenchyma (intratumoral), has been shown to be clinically significant, stromal and intratumoral compartments were defined according to standardized methods before lymphocyte counting (25). Quantitative analyses of lymphocytes or macrophages was performed at high power (×200) by counting the total number of cells within three separate areas each measuring 1 mm^2. The average number of cells per square millimeter was then calculated. The stromal and intratumoral compartments were both analyzed separately, and cells per square millimeter are reported (D.J.T.).

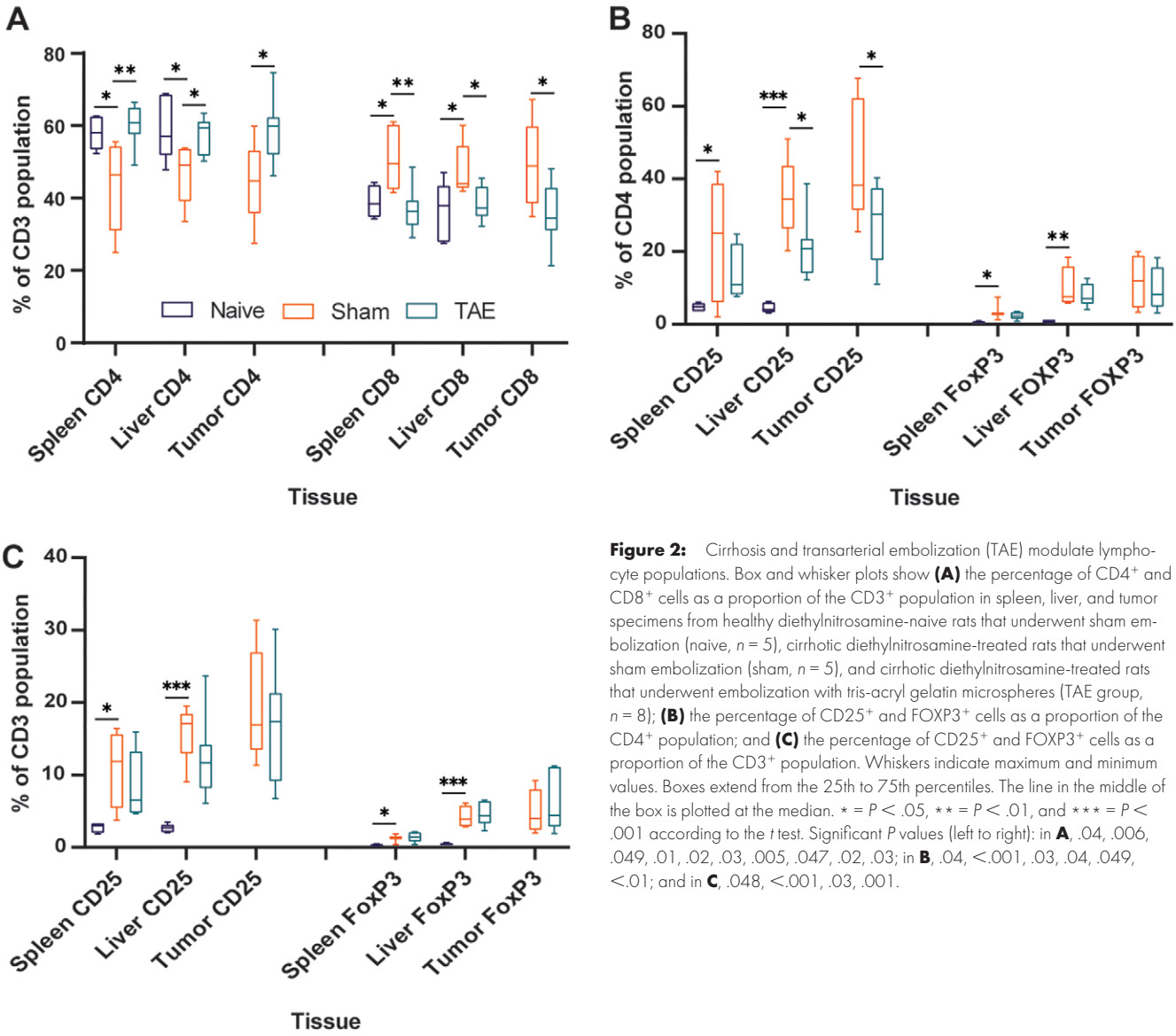

Figure 2: Cirrhosis and transarterial embolization (TAE) modulate lymphocyte populations. Box and whisker plots show **(A)** the percentage of CD4$^+$ and CD8$^+$ cells as a proportion of the CD3$^+$ population in spleen, liver, and tumor specimens from healthy diethylnitrosamine-naive rats that underwent sham embolization (naive, $n = 5$), cirrhotic diethylnitrosamine-treated rats that underwent sham embolization (sham, $n = 5$), and cirrhotic diethylnitrosamine-treated rats that underwent embolization with tris-acryl gelatin microspheres (TAE group, $n = 8$); **(B)** the percentage of CD25$^+$ and FOXP3$^+$ cells as a proportion of the CD4$^+$ population; and **(C)** the percentage of CD25$^+$ and FOXP3$^+$ cells as a proportion of the CD3$^+$ population. Whiskers indicate maximum and minimum values. Boxes extend from the 25th to 75th percentiles. The line in the middle of the box is plotted at the median. $*$ = $P < .05$, $**$ = $P < .01$, and $***$ = $P < .001$ according to the *t* test. Significant *P* values (left to right): in **A**, .04, .006, .049, .01, .02, .03, .005, .047, .02, .03; in **B**, .04, <.001, .03, .04, .049, <.01; and in **C**, .048, <.001, .03, .001.

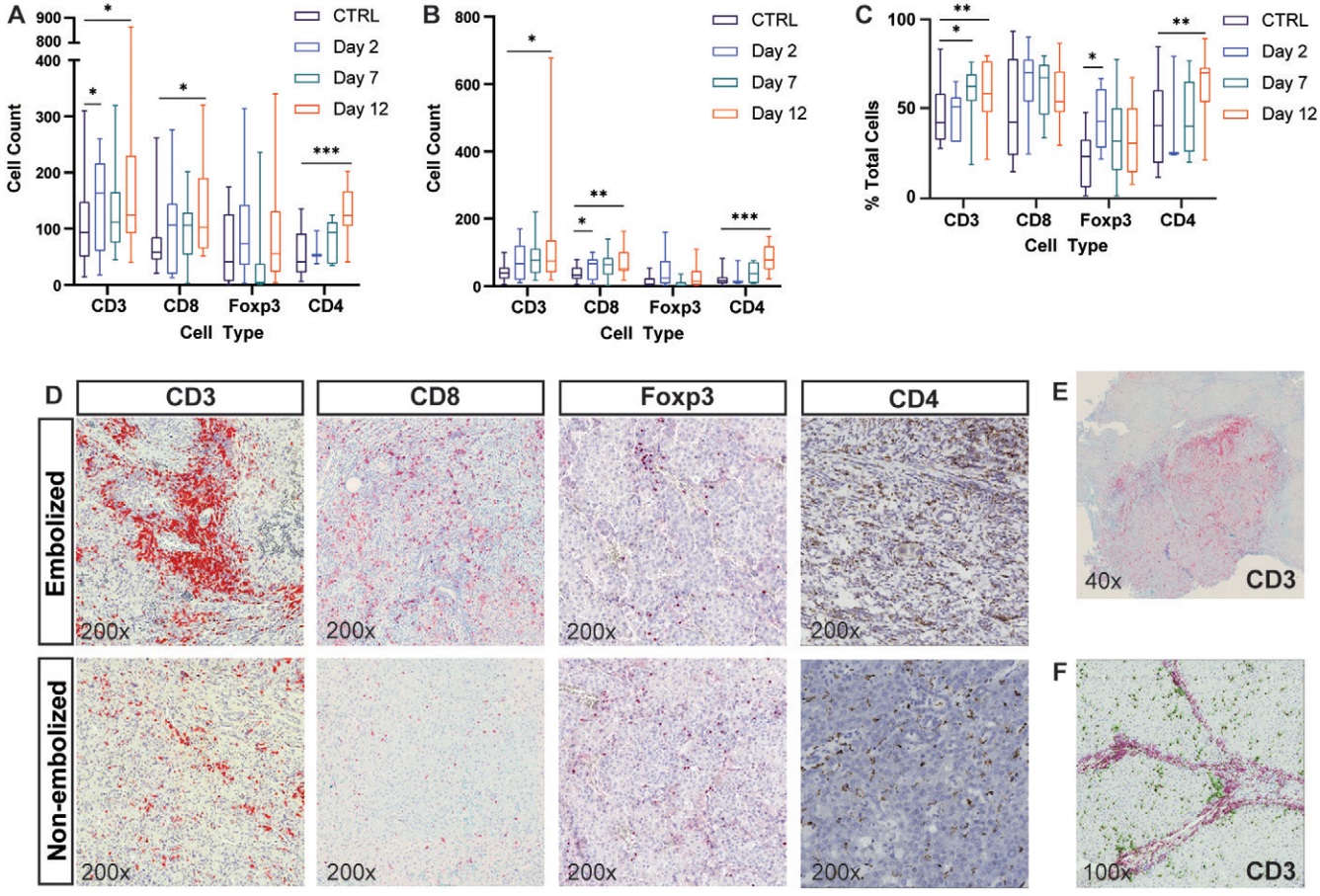

Figure 3: Transarterial embolization induces increased lymphocyte infiltration in embolized tumors. Box and whisker plots show **(A)** the average number of $CD3^+$, $CD8^+$, $FOXP3^+$, and $CD4^+$ cells (intrastromal and intratumoral cells) at 2 days ($n = 7$), 7 days ($n = 12$), and 12 days ($n = 17$) after embolization relative to control (CTRL) tumors that were not embolized ($n = 12$); **(B)** the average number of cells within the intratumoral compartment of embolized tumors at 2, 7, and 12 days after embolization relative to control tumors that were not embolized; and **(C)** the average percentage of immune cells found within the intratumoral compartment expressed as a percentage of total number of cells (intrastromal plus intratumoral cells) at 2, 7, and 12 days after embolization relative to control tumors that were not embolized. Whiskers indicate maximum and minimum values. Boxes extend from the 25th to 75th percentiles. The line in the middle of the box is plotted at the median. $* = P < .05$, $** = P < .01$, and $*** = P < .001$ according to the generalized estimating equation model. Significant P values (left to right): in **A**, .02, .03, .01, <.001; in **B**, .02, .02, .001, <.001; and in **C**, .02, .007, .01, .002. **(D)** Representative images of histologic staining of CD3, CD8, FOXP3, and CD4 cell markers in embolized and control tumors. **(E)** Representative low-magnification image shows $CD3^+$ cell infiltration into a hepatocellular carcinoma (HCC) tumor 12 days after embolization. **(F)** Representative image demonstrates intrastromal $CD3^+$ cells (pink markers) and intratumoral $CD3^+$ cells (green markers) within HCC specimens.

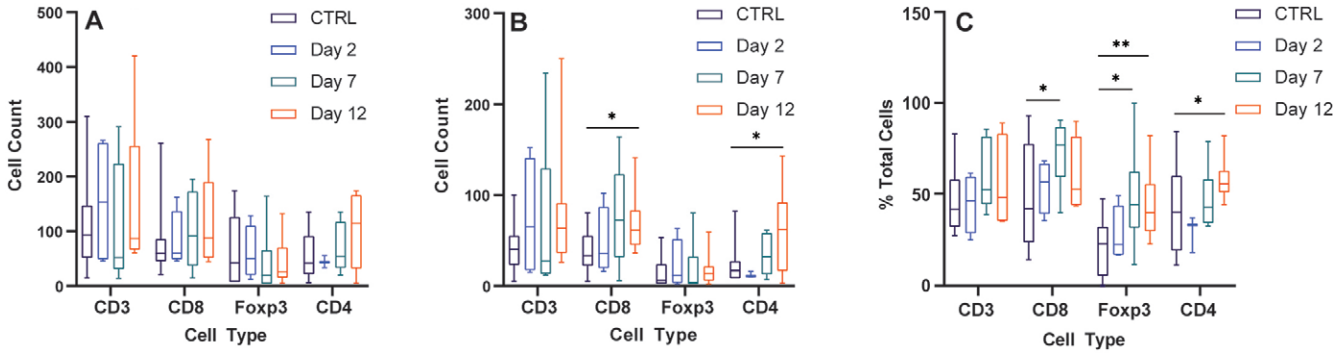

Figure 4: Transarterial embolization increases the number and proportion of tumor-infiltrating lymphocytes in the intratumoral compartment of nontarget tumors. Box and whisker plots show **(A)** the average number of $CD3^+$, $CD8^+$, $FOXP3^+$, and $CD4^+$ cells (intrastromal and intratumoral cells) at 2 days ($n = 4$), 7 days ($n = 6$), and 12 days ($n = 8$) after embolization in nontarget tumors relative to control (CTRL) tumors from rats that did not undergo embolization ($n = 12$); **(B)** the average number of cells within the intratumoral compartment of nontarget tumors at 2, 7, and 12 days after embolization relative to control tumors; and **(C)** the average percentage of cells found within the intratumoral compartment as a function of total number of cells (intrastromal plus intratumoral cells) in nontarget tumors at 2, 7, and 12 days after embolization relative to control tumors. Whiskers indicate maximum and minimum values. Boxes extend from the 25th to 75th percentiles. The line in the middle of the box is plotted at the median. $* = P < .05$ and $** = P < .01$ according to the generalized estimating equation model. Significant P values (left to right): in **B**, .02, .04; in **C**, .02, .03, .002, .01.

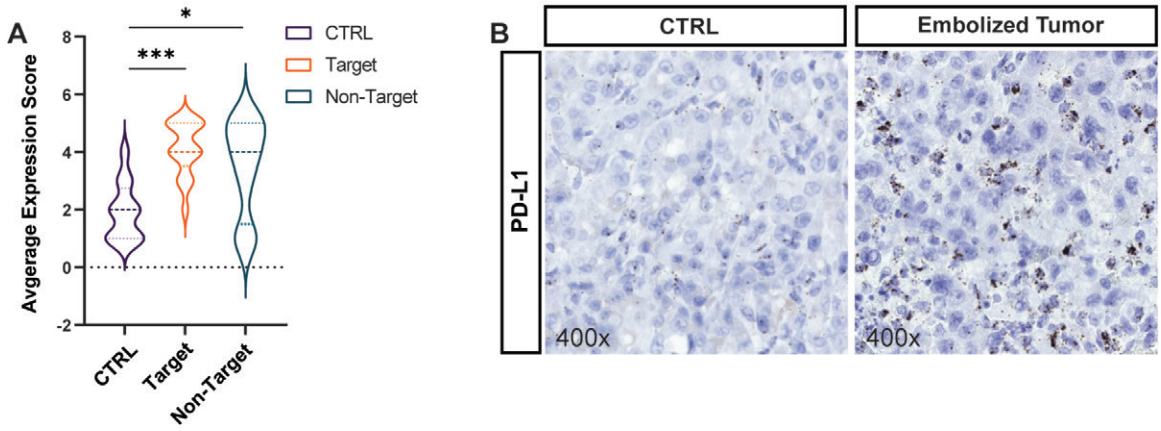

Figure 5: Transarterial embolization induces increased expression of programmed cell death protein ligand-1 (*PD-L1*) by hepatocellular carcinoma cells. **(A)** Violin plot shows the average expression score of *PD-L1* as determined with in situ hybridization (ISH) in untreated control tumors (CTRL) ($n = 12$), embolized tumors (target) ($n = 17$), and nontarget tumors ($n = 8$) in rats that underwent embolization. Tissues were collected for analysis 12 days after embolization. Bold dotted lines indicate medians, and thin dotted lines indicate quartiles. * = $P < .05$ and *** = $P < .001$ according to the general estimating equation model. Significant *P* values: <.001 (left), .02 (right). **(B)** Representative images of *PD-L1* ISH (3,3′-diaminobenzidine stain [brown stain]) in embolized tumors and untreated control tumors that were not embolized. Sections have been counterstained with hematoxylin to mark cell nuclei.

For embolic analyses in rat tissue, samples that had visible embolic particles were selected. To quantify peri-embolic leukocytes, a region of interest calculation was performed that encompassed a circumference twice the diameter of the embolic. Confluent embolics were considered to be a single "island" of embolic particles, and adjacent cells were counted together along with the number of embolic particles present. The maximum number of individually resolvable embolics within an "island" was 50, which was used as the cap when determining immune cell numbers on a per-embolic basis (D.J.T. and A.G.). To calculate CD68 response around embolics located in or out of vessels, region of interest analysis was applied as described earlier, and positive smooth muscle actin staining around embolic particles was used to indicate an intravascular location. See Appendix E1 (online) for additional details.

To determine whether embolic particles exhibit similar phenomena in human patients with HCC treated with TACE, we performed IHC for the general immune cell marker CD45 on human HCC samples from patients who had been treated with TACE using either TAGM or hydrogel embolics (Bead Block microspheres [predecessor of LUMI beads], BTG). Access to archived human HCC tissue specimens (four patients with a total of 240 embolic particles located intravascularly; five patients with a total of 142 embolic particles located extravascularly) received approval from our institutional review board on human research, and the requirement for informed consent was waived. See Appendix E1 (online) for additional details.

Statistical Analysis

Generalized estimating equation models were used to determine the impact of the predictors (day, embolic type, group) on outcome measures related to Figures 3–6 (SAS, version 9.4; SAS Institute). For Figures 3 and 4, our generalized estimating equation model included main effects for post-embolization time point and tumor group (target or nontarget), as well as an interaction term between the two. For Figures 5, 6, and 7C, the generalized estimating equation model was limited to main effects. Student *t* tests for the data included in Figure 2, Mann-Whitney *U* test for the data included in Figure 7E, χ^2 test for the data included in Figure 7B, and all graphs were performed or generated in GraphPad Prism 9.0 (GraphPad Software). All statistical tests used a cutoff of .05 to determine statistical significance. See Appendix E1 (online) for additional statistical details.

Data Availability

Data generated or analyzed during the study are available from the corresponding author by request.

Results

Cirrhosis and TAE Influence Intrahepatic Lymphocyte Populations

Relative to naive rats, sham-treated rats displayed a greater proportion of $CD8^+$, $CD25^+/CD4^+$, and $FOXP3^+$ lymphocytes in the liver (respectively, 36.1% vs 47.7% [$P = .047$]; 4.6% vs 34.9% [$P < .001$]; and 0.8% vs 9.8% [$P = .009$]) and spleen (39.0% vs 50.9% [$P = .03$]; 4.7% vs 22.9% [$P = .045$]; and 0.6% vs 3.9% [$P = .049$]), as well as a lower proportion of $CD4^+$ cells (liver, 59.6% vs 46.9% [$P = .049$]; spleen, 58.0% vs 43.4% [$P = .04$]) (Fig 2). When comparing TAE-treated rats to sham-treated rats, we observed a reduction in the proportion of $CD8^+$ cells within spleen, liver, and target tumor (spleen, 50.9% vs 36.7% [$P = .005$]; liver, 47.7% vs 38.4% [$P = .02$]; tumor, 49.1% vs 35.5% [$P = .03$]), with a corresponding increase in $CD4^+$ cells (spleen, 43.4% vs 60.2% [$P = .006$]; liver, 46.9% vs 57.6% [$P = .01$]; tumor, 44.5% vs 58.9% [$P = .02$]) (Fig 2A). In addition, TAE-treated rats demonstrated a reduction in the proportion of $CD25^+/CD4^+$ cells within the liver and target

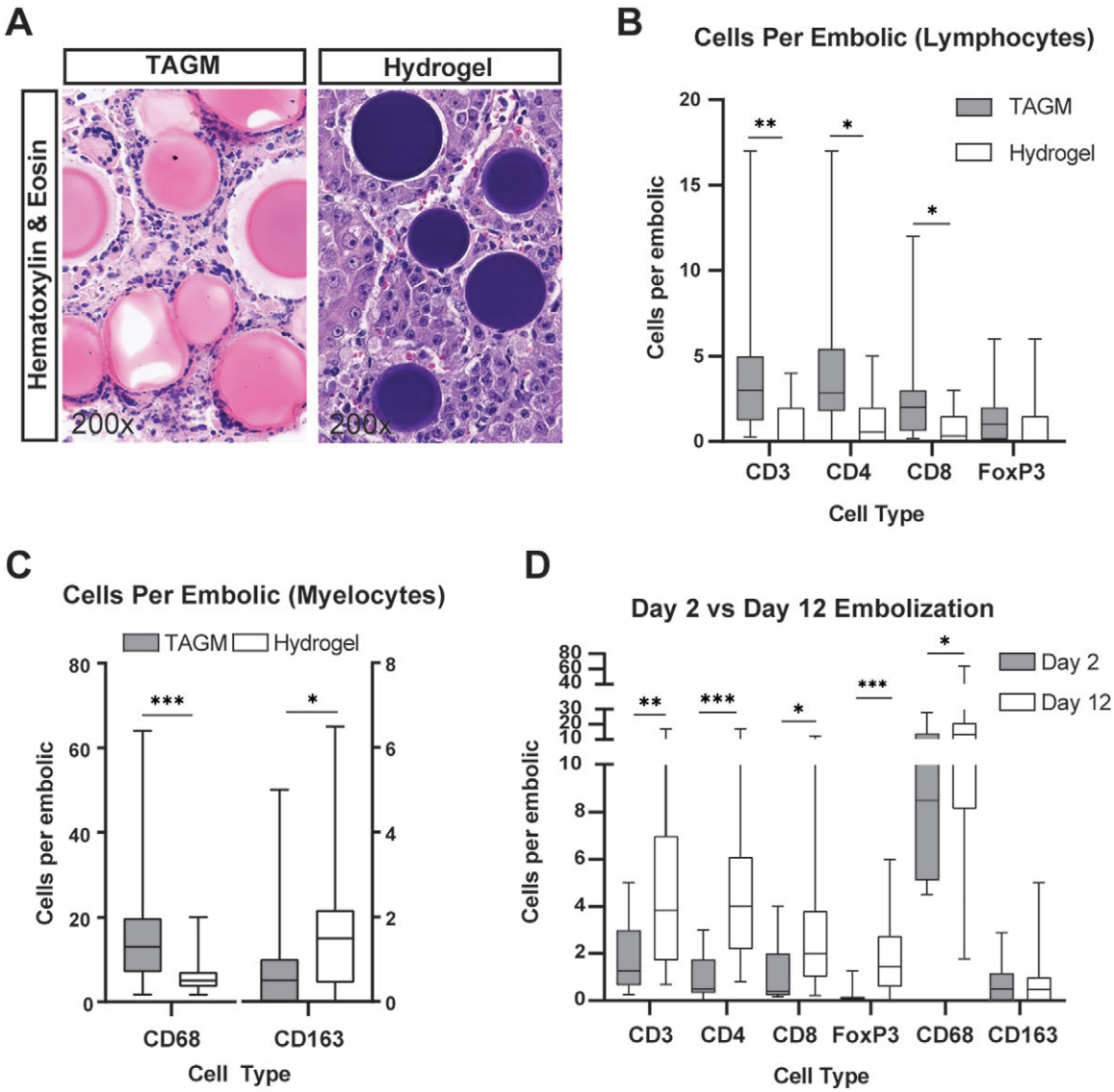

Figure 6: Recruitment of lymphocytes and myelocytes differed based on type of embolic. **(A)** Representative images of hematoxylin and eosin staining demonstrate differences in foreign body reactions induced within hepatocellular carcinoma tumors embolized with hydrogel embolics (hydrogel) or tris-acryl gelatin microspheres (TAGM). Because of their unique chemical properties, hydrogel embolics stain purple and TAGM stain pink when subjected to hematoxylin and eosin staining. Whereas numerous small-cell nuclei characteristic of immune cells can be seen surrounding TAGM, hydrogel embolics have relatively few immune cells associated with them (cell nuclei in proximity to hydrogel embolics largely reflect tumor cells). **(B–D)** Box and whisker plots show **(B)** the average number of $CD3^+$ (51 TAGM, 19 hydrogel), $CD4^+$ (46 TAGM, 24 hydrogel), $CD8^+$ (53 TAGM, 21 hydrogel), and $FOXP3^+$ (38 TAGM, 21 hydrogel) cells per embolic by embolic type; **(C)** the average number of $CD68^+$ (68 TAGM, 30 hydrogel) and $CD163^+$ (79 TAGM, 29 hydrogel) macrophages per embolic by embolic type; and **(D)** the average number of cells surrounding TAGM at 2 and 12 days after embolization. Whiskers indicate maximum and minimum values. Boxes extend from the 25th to 75th percentiles. The line in the middle of the box is plotted at the median. * = $P < .05$, ** = $P < .01$, and *** = $P < .001$ according to the generalized estimating equation model. Significant *P* values (left to right): in **B**, .003, .01, .03; in **C**, <.001, .03; and in **D**, .003, <.001, .04, <.001, .04.

tumor relative to sham-treated rats (34.9% vs 21.1% [$P = .03$]; 45.1% vs 27.5% [$P = .04$]) (Fig 2B).

TAE Enhances Recruitment of TILs

We compared the average number of lymphocytes (intratumoral plus intrastromal) per square millimeter within untreated tumors with embolized tumors at postembolization days 2, 7, and 12. Within embolized tumors, there were greater numbers of $CD3^+$, $CD4^+$, and $CD8^+$ TILs at 12 days after embolization relative to untreated controls (191.4 cells/mm^2 vs 106.7 cells/mm^2 [$P = .03$]; 127.8 cells/mm^2 vs 53.8 cells/mm^2 [$P < .001$]; and 131.4 cells/mm^2 vs 78.3 cells/mm^2 [$P = .01$]) (Fig 3A, 3D, 3E). Next, we examined the average number and proportion of lymphocytes in the intratumoral compartment. Consistent with the aforementioned results, we found a greater number of $CD3^+$, $CD4^+$, and $CD8^+$ cells within the intratumoral compartment at 12 days after embolization relative to control tumors (123.9 cells/mm^2 vs 45.3 cells/mm^2 [$P = .02$]; 80 cells/mm^2 vs 22.3 cells/mm^2 [$P < .001$]; and 71.9 cells/mm^2 vs 35.9 cells/mm^2

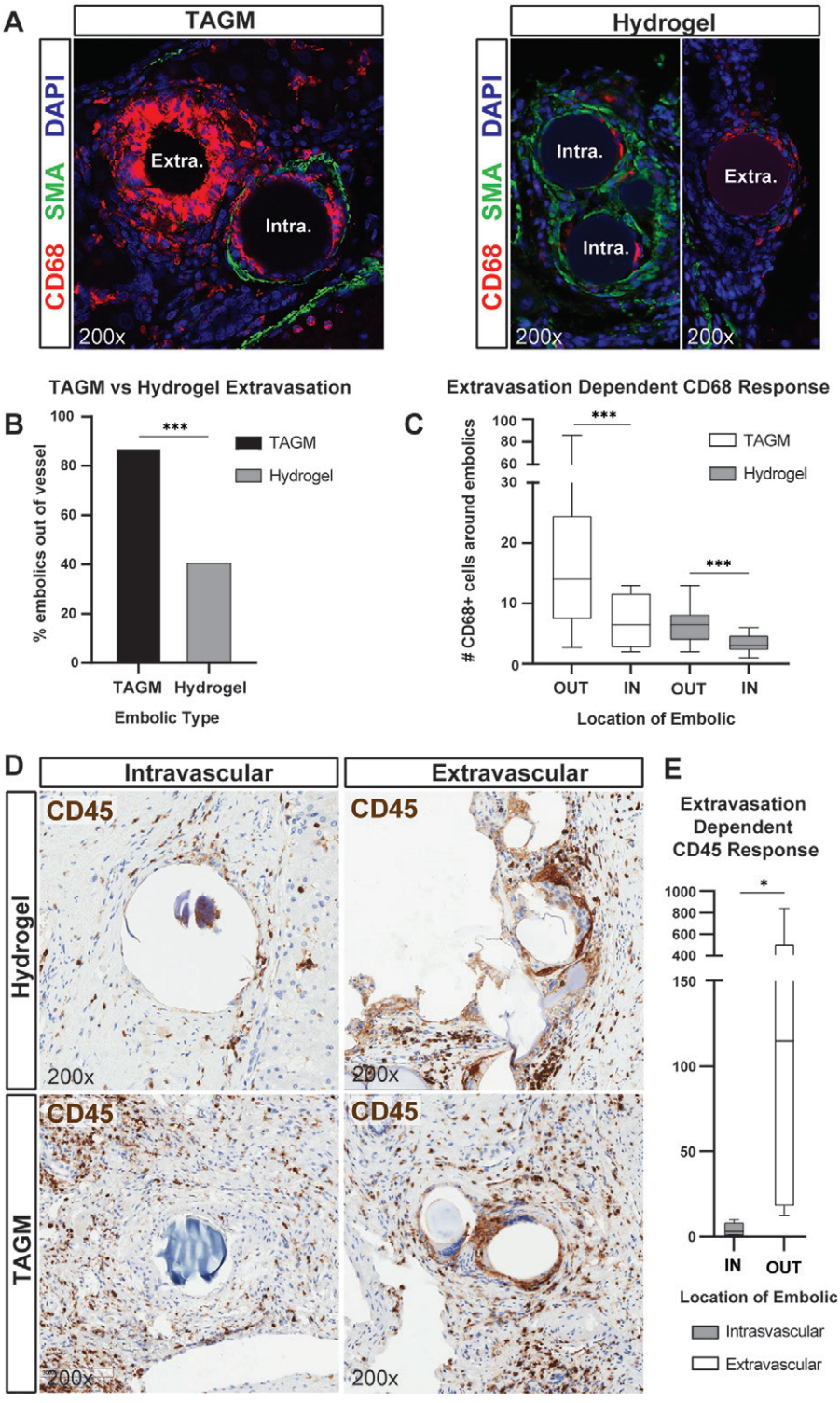

Figure 7: Tris-acryl gelatin microspheres (TAGM) induce a marked foreign body reaction that increases with extravasation. **(A)** Representative images show triple immunofluorescence for the macrophage marker CD68, arterial marker smooth muscle actin (SMA), and 4′,6-diamidino-2-phenylindole (DAPI) stain (marks cell nuclei) on hepatocellular carcinoma (HCC) specimens containing hydrogel embolics or TAGM. The foreign body reaction, as indicated by macrophage number, differs between embolic type and vascular location. Extra = extravascular, Intra = intravascular. **(B)** Bar graph shows the percentage of embolic particles found within smooth muscle actin–positive vascular walls by embolic type. **(C)** Box and whisker plot shows the average number of $CD68^+$ macrophages surrounding hydrogel embolics (14 outside, 20 inside) and TAGM (41 outside, six inside) based on vascular location. Whiskers indicate maximum and minimum values. Boxes extend from the 25th to 75th percentiles. The line in the middle of the box is plotted at the median. **(D)** Representative images of CD45 immunohistochemistry (3,3′-diaminobenzidine [DAB] stain [brown stain]) on posttransarterial chemoembolization human HCC specimens co-stained with hematoxylin. For illustrative purposes, images of hydrogel embolics (100–300 μm in size) and TAGM (100–300 μm in size) are shown in both intravascular and extravascular locations, as annotated. **(E)** Box and whisker plot shows the average number of surrounding $CD45^+$ cells per embolic particle based on vascular location (four patients with a total of 240 particles located intravascularly; five patients with a total of 142 particles located extravascularly). * = $P < .05$ and *** = $P < .001$ according to the χ^2 test for **B**, generalized estimating equation model for **C**, and Mann-Whitney *U* test for **E**. Significant *P* values (left to right): in **B**, <.001; in **C**, <.001, <.001; and in **E**, .02.

[P = .001], respectively) (Fig 3B, 3F). When comparing differences in the proportions of cells found within the intratumoral compartment, we found a greater proportion of CD3 and CD4 cells at 12 days after embolization relative to controls (58.5% vs 45.3% [P = .007]; 62.4% vs 41.9% [P = .002]), as well as an increased proportion of FOXP3 cells within the intratumoral compartment at 2 days after embolization (43.6% vs 21.0% [P = .01]) that did not persist at 7 (34.0% vs 21.0% [P = .25]) or 12 days (32.5% vs 21.0% [P = .12]) (Fig 3C).

TAE Increases the Number of TILs in the Intratumoral Compartment of Nontarget Tumors and Modulates *PD-L1* Expression

Within embolized rats that had at least one nontargeted tumor, we found no difference in the average number of $CD3^+$, $CD4^+$, $CD8^+$, and $FOXP3^+$ TILs within the entire nontarget tumor at any of the time points studied (CD3: 106.7 cells/mm^2 [control] vs 154.3 [day 2, P = .35], 107.5 [day 7, P = .97], and 157.5 [day 12, P = .27]; CD4: 53.8 cells/mm^2 vs 43.7 [P = .49], 68.5 [P = .53], and 104.3 [P = .12]; CD8: 78.3 cells/mm^2 vs 81.5 [P = .91], 100.2 [P = .46], and 123.3 [P = .18]; FOXP3: 65.1 cells/mm^2 vs 60.0 [P = .83], 40.3 [P = .34], and 44.0 [P = .24]) (Fig 4A). However, nontarget tumors demonstrated a greater number of $CD4^+$ and $CD8^+$ TILs in the in-

tratumoral compartment at day 12 relative to untreated controls (63.6 vs 22.3 cells/mm^2 [P = .04]; 68.7 vs 35.9 cells/mm^2 [P = .02]) (Fig 4B). Differences in the proportions of TILs within the intratumoral compartment of nontarget lesions as compared with controls were heterogeneous, with a greater proportion of CD8$^+$ TILs at day 7 (72.8% vs 49.4% [P = .02]), CD4$^+$ TILs at day 12 (58.1% vs 41.9% [P = .01]), and FOXP3$^+$ TILs at days 7 and 12 (48.1% vs 21.0% [P = .03]; 43.6% vs 21.0% [P = .002]) (Fig 4C).

Next, we sought to determine whether TAE influences the expression of *PD-L1* by HCC tumors in our rat model. Within embolized tumors, the average expression score of *PD-L1* was higher relative to controls (4.1 arbitrary units [au] vs 1.9 au [P < .001]). A smaller increase was observed within nontarget tumors compared with controls (3.5 au vs 1.9 au [P = .02]) (Fig 5).

Embolic Type and Vascular Location Influence Recruitment of Lymphocytes and Macrophages

Hematoxylin and eosin–stained sections demonstrated a strikingly greater number of inflammatory immune cells encircling TAGM compared with hydrogel embolics (Fig 6A). These findings were confirmed at quantitative analysis of IHC and ISH, which demonstrated a greater number of CD3$^+$, CD4$^+$, and CD8$^+$ lymphocytes in proximity to TAGM as compared with hydrogel embolics (4.1 vs 2.0 [P = .003]; 3.7 vs 2.0 [P = .01]; 2.2 vs 1.1 [P = .03]) (Fig 6B). Similarly, IHC demonstrated a markedly greater number of CD68$^+$ cells around TAGM (13.6 vs 5.8 [P < .001]) (Fig 6C). The number of immune cells encircling embolic particles on day 2 versus day 12 was also compared (Fig 6D).

To compare the influence of intra- versus extravascular location of the embolic agent on macrophage recruitment, we performed immunofluorescence for the general macrophage marker CD68 and the vascular marker smooth muscle actin (Fig 7A). Quantitative analysis revealed that TAGM extravasated at higher rates as compared with hydrogel embolics (87.4% vs 41.2% [P < .001]) (Fig 7B). Interestingly, extravasated embolic particles recruited greater numbers of CD68$^+$ macrophages as compared with embolic particles that remained within the intravascular space (17.9 extravascular CD68$^+$ peri-TAGM cells vs 7.0 intravascular CD68$^+$ peri-TAGM cells [P < .001]; 6.4 CD68$^+$ extravascular peri-hydrogel embolic cells vs 3.4 CD68$^+$ intravascular peri-hydrogel embolic cells [P < .001]) (Fig 7A, 7C).

Similar analysis of human HCC tumors following TACE demonstrated that TAGM and hydrogel embolics were identified both intra- and extravascularly within embolized tumors (Fig 7D). Consistent with our findings in rats, extravasated embolic particles recruited a greater number of CD45$^+$ immune cells as compared with embolic particles that remained within the intravascular compartment (four vs 231 [P = .02]) (Fig 7D, 7E).

Discussion

Clinical trials are underway to test the presumed benefit of combinations of locoregional and immunotherapies (22,26–28). However, data characterizing the influence of embolotherapy on the immune landscape remain lacking. Herein, we demonstrated that transarterial embolization dynamically influences the number and ratio of effector T cells within the tumor microenvironment of target and nontarget tumors (CD3: 191.4 cells/mm^2 vs 106.7 cells/mm^2 [P = .03]; CD4: 127.8 vs 53.8 [P < .001]; CD8: 131.4 vs 78.3 [P = .01]) and that *PD-L1* expression is higher in both target and nontarget tumors (target: 4.1 au vs 1.9 au [P < .001]; nontarget: 3.5 au vs 1.9 au [P = .02]). In addition, we demonstrated the impact of embolic type (per-embolic CD3: tris-acryl gelatin microspheres [TAGM] vs hydrogel embolics, 4.1 vs 2.0 [P = .003]; CD4: 3.7 vs 2.0 [P = .01]; CD8: 2.2 vs 1.1 [P = .03]) and vascular location (17.9 extravascular CD68$^+$ peri-TAGM cells vs 7.0 intravascular CD68$^+$ peri-TAGM cells [P < .001]; 6.4 extravascular CD68$^+$ peri-hydrogel embolic cells vs 3.4 intravascular CD68$^+$ peri-hydrogel embolic cells [P < .001]; human CD45$^+$ cells, four intravascular vs 231 extravascular [P = .02]) on immune cell recruitment, with striking differences in the resulting immunomodulation in both rat and human hepatocellular carcinomas.

Prior studies examining the impact of TAE on TILs have also demonstrated significant alterations in the tumor immune microenvironment (10,20). Our study builds on this prior research, applying an autochthonous animal model together with ISH/IHC and flow cytometry to comprehensively measure multiple immune cell populations at multiple time points following embolization within tumor parenchyma (intratumoral) and tumor stroma (intrastromal). The observation that cirrhosis, a key component in the pathogenesis of most human HCCs, causes significant changes in the underlying tumor immune microenvironment suggests the relevance of this model for the study of certain aspects of HCC immunobiology (29–31). Furthermore, studies in human patients with HCC have demonstrated striking correlations between certain molecular subtypes and the immunologic landscape. For example, tumor-intrinsic active β-catenin, or *CTNNB1*, signaling has been shown to result in T-cell exclusion and resistance to ICIs (32). Similar to human HCC, diethylnitrosamine-induced HCC tumors arise from a heterogeneous array of driver mutations, approximately half of which have been identified in human HCC samples, including *TP53* and *CTNNB1* (33). Moreover, autochthonous tumors have been shown to most closely recapitulate the biologic characteristics of the tumor microenvironment, including vasculature, immunobiologic characteristics, and architecture (34,35). Specifically, the dependence of HCC on the arterial blood supply develops over time through the growth of abnormal intranodular arteries, a characteristic that distinguishes autochthonous from transplanted tumor models and is particularly relevant in the study of embolotherapy (36,37). Indeed, the observed extravasation of embolic particles is likely to be influenced by the unique structural features of intratumoral arteries. The demonstration of this phenomenon in clinical samples further emphasizes the translational relevance of this model.

Clinical studies examining the role of TACE in modulating the anti-HCC immune response have been limited by the dearth of tissue samples from treated tumors and heterogeneity in embolization protocols, including the choice of embolic agent. Hematoxylin and eosin staining revealed dramatically different foreign body responses in HCCs treated with hydrogel embolics as compared with TAGM. Further analysis demonstrated

significant differences in the quantity of lymphocytes and myelocytes attracted to each type of embolic agent. These results underscore differences in how embolic agents access and engage the immune system based on vascular location. Interestingly, the data reported herein indicate that extravasation may be an advantageous phenomenon that can be harnessed to enhance antitumor immunity. Further studies are required to explore factors influencing this extravasation and the observed differences in the surrounding immune response, which may include the concentration, material composition, and/or size of the embolic agents and the role of pressure-enhanced delivery (38–41). These findings also underscore the potential for the development of designer embolic particles that integrate therapies or coatings capable of polarizing the antitumor immune response.

Finally, the described findings hold important implications given the completed (8,9) and ongoing clinical trials investigating the use of TACE in combination with ICIs for the treatment of HCC (Table E2 [online]). In addition to demonstrating the temporal changes in the immune response induced by TAE, we found that TAE causes increased expression of *PD-L1* in both target and nontarget tumors consistent with recent findings in human tissue samples (23). These data reaffirm the notion that combination therapy with programmed cell death protein 1 or PD-L1 inhibitors may act synergistically to overcome the seemingly negative consequence of increased *PD-L1* expression on tumor cells, which might otherwise promote T-cell exhaustion; however, ICIs have also been associated with immune-related adverse reactions that can sometimes be fatal. Our study emphasizes the importance of a thorough understanding of the immune response to TAE as well as the timing and method of ICI administration, both to optimize treatment response and minimize adverse reactions.

Our study has several limitations. Due to the nature in which our samples were collected, quantitative measures of immune cell numbers were not obtained using stereologic methods, which may influence precision in counting. Furthermore, we only examined the impact of bland embolization on the immune response, and thus, it is unknown how the addition of chemotherapeutic agents might affect these results. In addition, the time of liver harvest for the human samples was not standardized, likely contributing to the observed variability across samples. Moreover, our choice of embolic agents was based on standard clinical protocols at our institution; it is unknown how differences in the size of human and rat vasculature alter the functionality of these particles. Finally, while the diethylnitrosamine rat model recapitulates the hepatic cirrhosis and disease progression observed in patients, the underlying causes of the liver disease in patients are heterogeneous, including exogenous or toxic, infectious, toxic or allergic, immunopathologic or autoimmune, and vascular processes that may have differential effects on the HCC immune microenvironment. As a result, our findings may not be generalizable to all of these patient populations.

In summary, our study delineates the dynamic transarterial embolization–induced cellular immune response in hepatocellular carcinoma. The data demonstrate the potential of locoregional embolotherapy to modulate the tumor immune microenvironment directly and provide unique insights into the nature, breadth, and mechanism of the induced alterations. These findings hold important implications for the ongoing development of therapeutic strategies combining locoregional therapy with immunomodulators as well as for the development of techniques and materials that further leverage the transarterial chemoembolization–induced modulation of the tumor immune microenvironment.

Author contributions: Guarantors of integrity of entire study, **D.J.T., A.G., D.E.K., T.P.F.G.**; study concepts/study design or data acquisition or data analysis/interpretation, all authors; manuscript drafting or manuscript revision for important intellectual content, all authors; approval of final version of submitted manuscript, all authors; agrees to ensure any questions related to the work are appropriately resolved, all authors; literature research, **D.J.T., A.G., G.J.N., E.F., S.J.H., T.P.F.G.**; clinical studies, **D.J.T., G.J.N., E.F., S.J.H.**; experimental studies, **D.J.T., A.G., O.J., I.G., G.J.N., E.F., S.J.H., T.P.F.G.**; statistical analysis, **D.J.T., A.G., I.G., D.E.K., E.F., T.P.F.G.**; and manuscript editing, **D.J.T., A.G., O.J., G.J.N., M.C.S., D.E.K., E.F., S.J.H., T.P.F.G.**

Acknowledgments: The authors thank Scott Appel, MS, co-director of the Biostatistics Analysis Center at the University of Pennsylvania, for his help in generating the generalized estimating equation model used in this study, as well as for statistical advice. In addition, the authors thank the Molecular Pathology and Imaging Core for their technical assistance in preparing samples for histologic analyses.

Disclosures of conflicts of interest: **D.J.T.** No relevant relationships. **A.G.** No relevant relationships. **O.J.** No relevant relationships. **I.G.** No relevant relationships. **G.J.N.** No relevant relationships. **M.C.S.** Grants from Guerbet, Sirtex, and Pfizer; consulting fees from Genentech and Instylla; leadership roles in the Society of Interventional Oncology and North American Neuroendocrine Tumor Society. **D.E.K.** Grants from Gilead, Bayer, and Glycotest; patent planned, issued, or pending for glypican-3 single-chain variable fragment and the uses thereof; American Association for the Study of Liver Diseases Foundation Research Award Committee chairperson. **E.F.** No relevant relationships. **S.J.H.** Research grant from the Society of Interventional Radiology; consulting fees from Boston Scientific; payment for lectures from Boston Scientific; member of the Society of Interventional Oncology immuno-oncology task force grant committee. **T.P.F.G.** Consulting fees from TriSalus Life Sciences and Instylla; payment for lectures from TriSalus Life Sciences and the Society for Interventional Oncology; payment for participation on a data safety monitoring or advisory board for TriSalus Life Sciences; chair of the Society for Interventional Oncology Research Committee and co-lead for the Society for Interventional Radiology National Institutes of Health Task Force (no payment received); institution received equipment, materials, or other services from Instylla.

References

1. Bray F, Ferlay J, Soerjomataram I, Siegel RL, Torre LA, Jemal A. Global cancer statistics 2018: GLOBOCAN estimates of incidence and mortality worldwide for 36 cancers in 185 countries. CA Cancer J Clin 2018;68(6):394–424 [Published correction appears in CA Cancer J Clin 2020;70(4):313.].
2. Surveillance Epidemiology and End Results Program. Liver and Intrahepatic Bile Duct Cancer. Cancer Stat Facts. https://seer.cancer.gov/statfacts/html/livibd.html. Published 2019. Accessed January 5, 2021.
3. Jin YJ, Chung YH, Kim JA, et al. Predisposing factors of hepatocellular carcinoma recurrence following complete remission in response to transarterial chemoembolization. Dig Dis Sci 2013;58(6):1758–1765.
4. Takayasu K, Arii S, Ikai I, et al. Prospective cohort study of transarterial chemoembolization for unresectable hepatocellular carcinoma in 8510 patients. Gastroenterology 2006;131(2):461–469.
5. Chu KF, Dupuy DE. Thermal ablation of tumours: biological mechanisms and advances in therapy. Nat Rev Cancer 2014;14(3):199–208.
6. Sidana A. Cancer immunotherapy using tumor cryoablation. Immunotherapy 2014;6(1):85–93.
7. Ayaru L, Pereira SP, Alisa A, et al. Unmasking of alpha-fetoprotein-specific CD4(+) T cell responses in hepatocellular carcinoma patients undergoing embolization. J Immunol 2007;178(3):1914–1922.
8. Agdashian D, ElGindi M, Xie C, et al. The effect of anti-CTLA4 treatment on peripheral and intra-tumoral T cells in patients with hepatocellular carcinoma. Cancer Immunol Immunother 2019;68(4):599–608.

9. Duffy AG, Ulahannan SV, Makorova-Rusher O, et al. Tremelimumab in combination with ablation in patients with advanced hepatocellular carcinoma. J Hepatol 2017;66(3):545–551.
10. Avritscher R, Jo N, Polak U, et al. Hepatic arterial bland embolization increases Th17 cell infiltration in a syngeneic rat model of hepatocellular carcinoma. Cardiovasc Intervent Radiol 2020;43(2):311–321.
11. Greten TF, Mauda-Havakuk M, Heinrich B, Korangy F, Wood BJ. Combined locoregional-immunotherapy for liver cancer. J Hepatol 2019;70(5):999–1007.
12. Keenan BP, Fong L, Kelley RK. Immunotherapy in hepatocellular carcinoma: the complex interface between inflammation, fibrosis, and the immune response. J Immunother Cancer 2019;7(1):267.
13. Knolle PA, Thimme R. Hepatic immune regulation and its involvement in viral hepatitis infection. Gastroenterology 2014;146(5):1193–1207.
14. Bilbao JI, de Luis E, García de Jalón JA, et al. Comparative study of four different spherical embolic particles in an animal model: a morphologic and histologic evaluation. J Vasc Interv Radiol 2008;19(11):1625–1638.
15. Stampfl U, Stampfl S, Bellemann N, et al. Experimental liver embolization with four different spherical embolic materials: impact on inflammatory tissue and foreign body reaction. Cardiovasc Intervent Radiol 2009;32(2):303–312.
16. Verret V, Wassef M, Pelage JP, et al. Influence of degradation on inflammatory profile of polyphosphazene coated PMMA and trisacryl gelatin microspheres in a sheep uterine artery embolization model. Biomaterials 2011;32(2):339–351.
17. Gade TPF, Hunt SJ, Harrison N, et al. Segmental transarterial embolization in a translational rat model of hepatocellular carcinoma. J Vasc Interv Radiol 2015;26(8):1229–1237.
18. Kiefer RM, Hunt SJ, Pulido S, et al. Relative initial weight is associated with improved survival without altering tumor latency in a translational rat model of diethylnitrosamine-induced hepatocellular carcinoma and transarterial embolization. J Vasc Interv Radiol 2017;28(7):1043–1050.e2.
19. Kumagai K, Horikawa M, Yamada K, Uchida BT, Farsad K. Transtail artery access in rats: a new technique for repeatable selective angiography. J Vasc Interv Radiol 2020;31(4):678–681.e4.
20. Duan XH, Li TF, Zhou GF, et al. Transcatheter arterial embolization combined with radiofrequency ablation activates $CD8^+$ T-cell infiltration surrounding residual tumors in the rabbit VX2 liver tumors. OncoTargets Ther 2016;9:2835–2844.
21. Takaki H, Imai N, Thomas CT, et al. Changes in peripheral blood T-cell balance after percutaneous tumor ablation. Minim Invasive Ther Allied Technol 2017;26(6):331–337.
22. Yarchoan M, Xing D, Luan L, et al. Characterization of the immune microenvironment in hepatocellular carcinoma. Clin Cancer Res 2017;23(23):7333–7339.
23. Montasser A, Beaufrère A, Cauchy F, et al. Transarterial chemoembolization enhances programmed death 1 and programmed death-ligand 1 expression in hepatocellular carcinoma. Histopathology 2021;79(1):36–46.
24. Wiede F, Tiganis T. Isolation and characterization of mouse intrahepatic lymphocytes by flow cytometry. Methods Mol Biol 2018;1725:301–311.
25. Hendry S, Salgado R, Gevaert T, et al. Assessing tumor-infiltrating lymphocytes in solid tumors: a practical review for pathologists and proposal for a standardized method from the International Immuno-Oncology Biomarkers Working Group: part 2: TILs in melanoma, gastrointestinal tract carcinomas, non-small cell lung carcinoma and mesothelioma, endometrial and ovarian carcinomas, squamous cell carcinoma of the head and neck, genitourinary carcinomas, and primary brain tumors. Adv Anat Pathol 2017;24(6):311–335.
26. Hiroishi K, Eguchi J, Baba T, et al. Strong CD8(+) T-cell responses against tumor-associated antigens prolong the recurrence-free interval after tumor treatment in patients with hepatocellular carcinoma. J Gastroenterol 2010;45(4):451–458.
27. Ding W, Xu X, Qian Y, et al. Prognostic value of tumor-infiltrating lymphocytes in hepatocellular carcinoma: a meta-analysis. Medicine (Baltimore) 2018;97(50):e13301.
28. Ghavimi S, Apfel T, Azimi H, Persaud A, Pyrsopoulos NT. Management and treatment of hepatocellular carcinoma with immunotherapy: a review of current and future options. J Clin Transl Hepatol 2020;8(2):168–176.
29. Albillos A, Lario M, Álvarez-Mon M. Cirrhosis-associated immune dysfunction: distinctive features and clinical relevance. J Hepatol 2014;61(6):1385–1396.
30. Sipeki N, Antal-Szalmas P, Lakatos PL, Papp M. Immune dysfunction in cirrhosis. World J Gastroenterol 2014;20(10):2564–2577.
31. Noor MT, Manoria P. Immune dysfunction in cirrhosis. J Clin Transl Hepatol 2017;5(1):50–58.
32. Harding JJ, Nandakumar S, Armenia J, et al. Prospective genotyping of hepatocellular carcinoma: clinical implications of next-generation sequencing for matching patients to targeted and immune therapies. Clin Cancer Res 2019;25(7):2116–2126.
33. Chen Z, Li S, Shen M, et al. The mutational and transcriptional landscapes of hepatocarcinogenesis in a rat model. iScience 2020;23(11):101690.
34. Sikder H, Huso DL, Zhang H, et al. Disruption of Id1 reveals major differences in angiogenesis between transplanted and autochthonous tumors. Cancer Cell 2003;4(4):291–299.
35. Becher OJ, Holland EC. Genetically engineered models have advantages over xenografts for preclinical studies. Cancer Res 2006;66(7):3355–3358; discussion 3358–3359.
36. Matsui O. Imaging of multistep human hepatocarcinogenesis by CT during intra-arterial contrast injection. Intervirology 2004;47(3-5):271–276.
37. Falk P. Differences in vascular pattern between the spontaneous and the transplanted C3H mouse mammary carcinoma. Eur J Cancer Clin Oncol 1982;18(2):155–165.
38. Levy EB, Gacchina Johnson C, Jacobs G, et al. Direct quantification and comparison of intratumoral hypoxia following transcatheter arterial embolization of VX2 liver tumors with different diameter microspheres. J Vasc Interv Radiol 2015;26(10):1567–1573.
39. Stampfl S, Bellemann N, Stampfl U, et al. Inflammation and recanalization of four different spherical embolization agents in the porcine kidney model. J Vasc Interv Radiol 2008;19(4):577–586.
40. Stampfl S, Stampfl U, Bellemann N, et al. Immunohistochemical characterization of specific inflammatory tissue reactions following embolization with four different spherical agents in the minipig kidney model. J Vasc Interv Radiol 2009;20(7):936–945.
41. Namur J, Citron SJ, Sellers MT, et al. Embolization of hepatocellular carcinoma with drug-eluting beads: doxorubicin tissue concentration and distribution in patient liver explants. J Hepatol 2011;55(6):1332–1338.